

DEVELOPMENTAL BIOLOGY

Increased chromatin accessibility promotes the evolution of a transcriptional silencer in *Drosophila*

Liucong Ling, Bettina Mühling, Rita Jaenichen, Nicolas Gompel*

The loss of discrete morphological traits, the most common evolutionary transition, is typically driven by changes in developmental gene expression. Mutations accumulating in regulatory elements of these genes can disrupt DNA binding sites for transcription factors patterning their spatial expression, or delete entire enhancers. Regulatory elements, however, may be silenced through changes in chromatin accessibility or the emergence of repressive elements. Here, we show that increased chromatin accessibility at the gene *yellow*, combined with the gain of a repressor site, underlies the loss of a wing spot pigmentation pattern in a *Drosophila* species. The gain of accessibility of this repressive element is regulated by E93, a transcription factor governing the progress of metamorphosis. This convoluted evolutionary scenario contrasts with the parsimonious mutational paths generally envisioned and often documented for morphological losses. It illustrates how evolutionary changes in chromatin accessibility may directly contribute to morphological diversification.

INTRODUCTION

The diversity of morphological characters in plants and animals breaks down into gains, losses, and modulation of traits. From a developmental standpoint, morphological characters of adult organisms are typically foreshadowed by discrete patterns of gene expression, driven by specific transcriptional enhancers during embryogenesis or postembryonic development (1–4). From an evolutionary standpoint, changes in these *cis*-regulatory elements drive changes in gene expression and thereby produce morphological variation (5). Consequently, the loss of a discrete trait, the most common evolutionary transition (6), often stems from the loss of function or deletion of enhancers underlying its formation (3, 7–9). The literature on enhancers and their evolution emphasizes their spatial activity and how transcription factor binding sites (TFBSs) for spatial regulators encode patterns (10–15). Recently, another aspect of enhancer biology has come under scrutiny, their accessibility (16, 17), reflecting the degree of local nucleosome occupancy and chromatin compaction. DNA accessibility of an enhancer is a prerequisite to the action of transcription factors (TFs) acting as spatial regulators (18). It is controlled during development by different parameters, including the action of pioneer TFs (19) and transcriptional activity per se (20, 21), and was shown to vary between species, along with TF binding (22). As such, the modulation of enhancer accessibility represents an obvious level of transcriptional regulation that could contribute to morphological divergence between species. We explored this possibility using a well-defined transcriptional enhancer associated with morphological evolution in *Drosophila*, the *spot* enhancer of the pigmentation gene *yellow* (8, 23–26). Several *Drosophila* species have patterns of black pigmentation on their wings, as, for instance, the wing-spotted fly *Drosophila biarmipes* (Fig. 1A). This character was gained once in a common ancestor of a species group containing *D. biarmipes* and the model species *Drosophila melanogaster*. It was subsequently lost several times in this group, including in *D.*

melanogaster itself (Fig. 1B) (8). The initial gain of a wing spot involved the co-option of *yellow*, a gene necessary for the production of black pigments, through the newly evolved *spot* regulatory activity (Fig. 1C) (23, 24). In at least one species from this group, *Drosophila gunungcola*, that lost its wing spot, the *spot* activity decayed through point mutations (8). Focusing on another species that has secondarily lost its wing spot (8), the model organism *D. melanogaster* itself, we investigated the evolution of accessibility of a regulatory region that has lost its enhancer activity.

RESULTS

Enhancer accessibility and enhancer activity show discrepancy at the *yellow* locus of *D. melanogaster*

To understand whether enhancer accessibility might also play a role in the loss of *spot* activity, we compared chromatin states at the *yellow* locus during wing pupal development between the spotted *D. biarmipes* and the nonspotted *D. melanogaster*. We first monitored the dynamic of *yellow* expression in developing wings of both species with quantitative polymerase chain reaction (qPCR) (fig. S1A) to facilitate the interpretation of accessibility. The two species showed marked differences in the expression dynamic, where *yellow* transcripts faded in *D. melanogaster* after 56% pupal development, while they slightly increased in *D. biarmipes*, in line with the *spot* activity (23). We then profiled accessibility upstream of *yellow* transcription at selected stages in the wings of both species using assay of transposase-accessible chromatin using sequencing (ATAC-seq) (Fig. 1, E and F, and fig. S1A) (27). At the onset of *yellow* expression (47% of pupal development), accessibility increased in both species with two adjacent peaks (Fig. 1F, peak-1 and peak-2), which tended to merge and fade at later stages. We were intrigued by two observations. First, the region of *D. melanogaster* orthologous to *D. biarmipes spot* enhancer (peak-1) (26) showed persistent accessibility throughout pupal development (Fig. 1F and fig. S1), although we detected no *spot* activity in *D. melanogaster* in a reporter assay ($y5^{mel}$; Fig. 1, D and E). We initially interpreted this as residual accessibility but found this unexpected, given that the wing spot was lost at least 10 million years ago in the

Copyright © 2023 The Authors, some rights reserved; exclusive licensee American Association for the Advancement of Science. No claim to original U.S. Government Works. Distributed under a Creative Commons Attribution NonCommercial License 4.0 (CC BY-NC).

Chair of Evolutionary Ecology, Ludwig-Maximilians Universität München, Faculty of Biology, Biozentrum, Grosshaderner Strasse 2, 82152 Planegg-Martinsried, Germany.

*Corresponding author. Email: gompel@bio.lmu.de

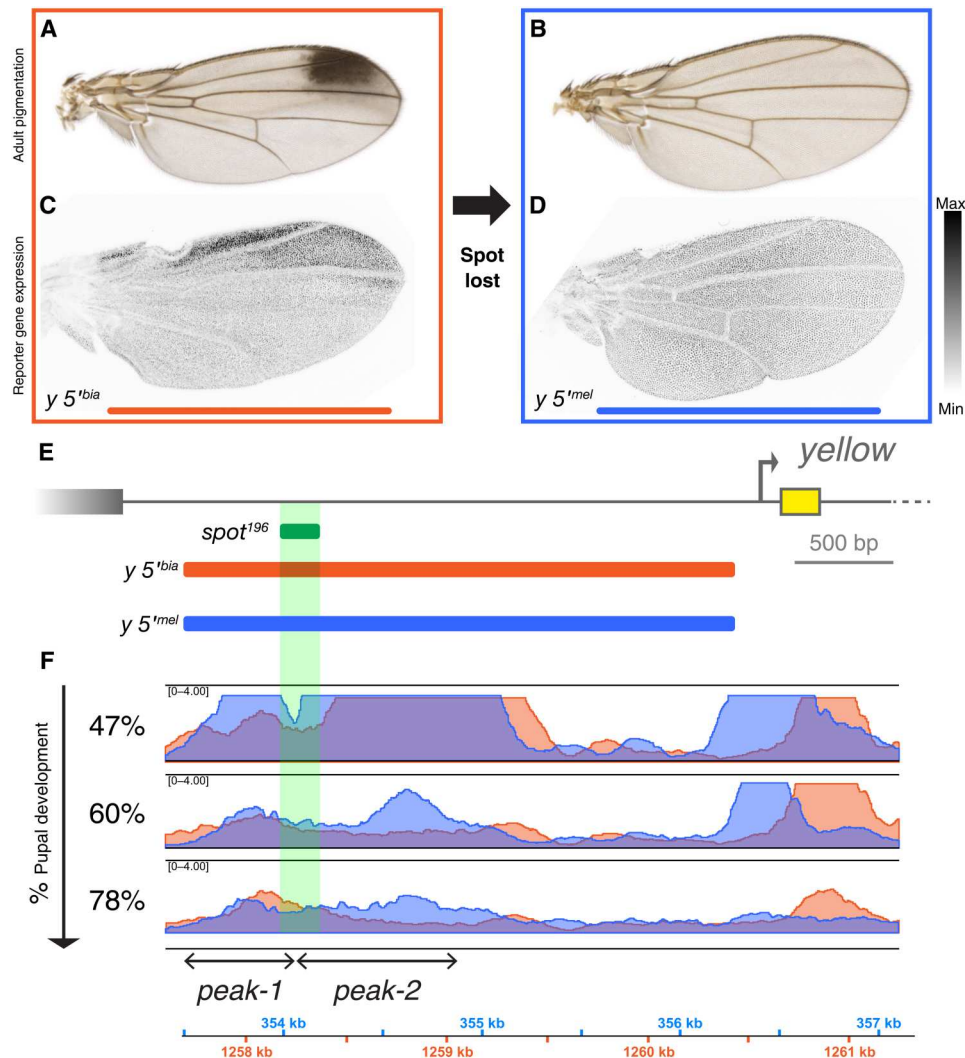


Fig. 1. Changes in accessibility in the regulatory regions of *yellow* associated with a loss in wing pigmentation. (A and B) Adult wings of *D. biarmipes* (A) and *D. melanogaster* (B). (C and D) Regulatory regions upstream of *yellow* transcription start site of *D. biarmipes* (C) and *D. melanogaster* (D) drive reporter expression in the wings of transgenic *D. melanogaster* at 80% of pupal development. The reporter activity levels foreshadow adult pigmentation of the respective species (see grayscale for fluorescence levels in all figures). (E) A map of the *yellow* locus indicates the relative positions of the fragments tested in (C) and (D) as well as the previously characterized *D. biarmipes* minimal enhancer *spot*¹⁹⁶ (23). bp, base pair. (F) Assay of transposase accessible chromatin sequencing (ATAC-seq) tracks of the corresponding *yellow* region from pupal wings at different stages (expressed in percentage of the pupal life duration). Note the presence of two peaks of accessibility, best separated at 47% of pupal development, a stage that we used to define the sequence coordinates of these peaks by visual inspection. Here and in all subsequent figures, the blue color denotes *D. melanogaster* and the orange color denotes *D. biarmipes*.

D. melanogaster lineage (8), leaving enough time to this DNA segment to lose accessibility. Second, we noted that peak-2 decreased largely in *D. biarmipes* after midpupal life (Fig. 1F and fig. S1A) but persisted in *D. melanogaster*, suggesting a possible link to the evolution of wing pigmentation (26).

A novel silencer and a cryptic enhancer underlie the loss of a wing spot in *D. melanogaster*

To understand the functional significance of these accessible regions, we derived a series of reporter constructs to assay the regulatory activities of the corresponding *D. melanogaster* sequences (Fig. 2, A to D). To our surprise, *D. melanogaster* sequences corresponding to peak-1 alone (construct *peak-1*^{mel}; Fig. 2C) drove

reporter expression in the spot region of the wing, in a spatial pattern comparable to the activity of the orthologous segment of *D. biarmipes* (23), albeit with weaker levels (fig. S3). We found that *peak-1*^{mel} activity depended on the TF Distal-less (Dll; fig. S2, A and B), as does *D. biarmipes* enhancer (23), confirming the functional orthology of these regulatory elements. This activity, however, was absent in a construct containing a fragment encompassing peak-1 and peak-2 [construct *peaks-(1+2)*^{mel}; Fig. 2B], which drove uniform wing expression resembling that of *y 5'*^{mel} (Fig. 1D). These results showed that the *spot* activity of *D. melanogaster* was not lost during evolution but instead became cryptic, masked by a repressive activity contained within peak-2 region.

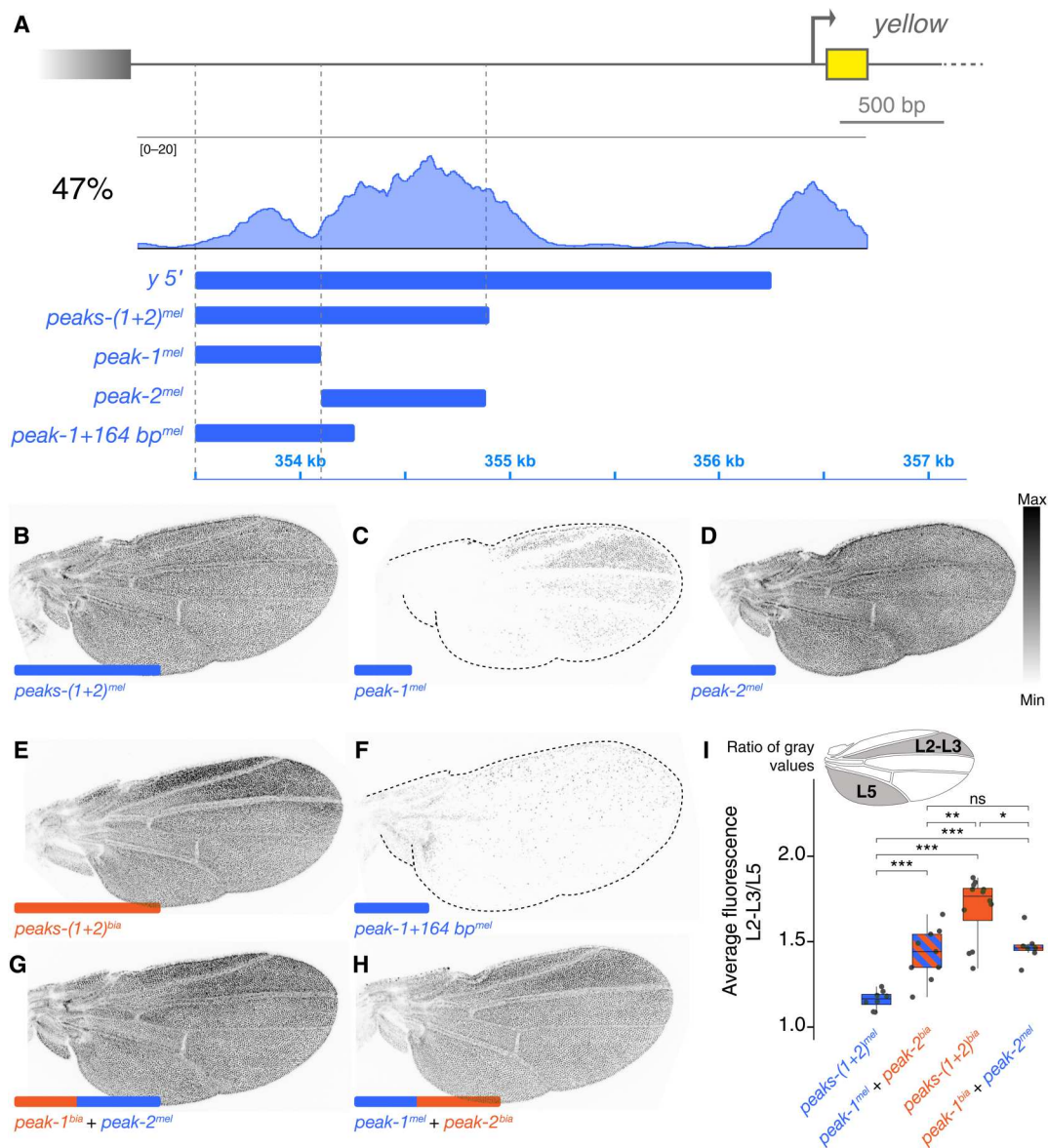


Fig. 2. A novel silencer represses the *spot* activity in *D. melanogaster*. (A) Design of reporter constructs to map the regulatory activities of accessible regions at the *yellow* locus of *D. melanogaster*. *peak-1* and *peak-2* segments were defined based on visual inspection of the accessibility profiles, rather than based on peak calling. (B to H) Reporter activity in transgenic *D. melanogaster* wings at 80% of pupal development for the following constructs: *peaks-(1+2)^{mel}* (B), *peak-1^{mel}* (C), *peak-2^{mel}* (D), *peaks-(1+2)^{bia}* (E), *peak-1+164 bp^{mel}* (F), *peak-1^{bia}+peak-2^{mel}* (G), and *peak-1^{mel}+peak-2^{bia}* (H). (I) Quantification of reporter activities in (B) to (H). Statistical differences were examined using the Wilcoxon test. All box plots show the median and first and third quartiles of the data, overlaid with individual data points. ns, not significant ($P > 0.05$); * $P < 0.05$; ** $P < 0.01$; *** $P < 0.001$. The contour of wings with weak reporter activity is identified with a dotted line. All wings in this figure are homozygous for the respective transgenes, and images were enhanced using the same settings, which differ from those used in other figures.

To test whether the observed repressive activity was specific to *D. melanogaster* or ancestral to both species, we used chimeric constructs. Specifically, we assayed the repressive effect of *D. melanogaster peak-2* (*peak-2^{mel}*) on *D. biarmipes spot* activity (*peak-1^{bia}*) and reciprocally (Fig. 2, E to H). A *peak-1^{bia}+peak-2^{mel}* construct resulted in reduced *spot* activity compared to a *peaks-(1+2)^{bia}* construct (Fig. 2, E, H, and I), indicating that the novel *cis*-repressing activity of *D. melanogaster* can target a heterologous *spot* enhancer. Conversely, while *D. melanogaster spot* enhancer was silenced in its original context [construct *peaks-(1+2)^{mel}*; Fig. 2B], it

became active when paired to *D. biarmipes peak-2* orthologous sequence (construct *peak-1^{mel}+peak-2^{bia}*; Fig. 2, H and I), confirming the absence of the repressive activity in *D. biarmipes peak-2*.

The DNA segment corresponding to *peak-2* overlaps with another enhancer, driving lower levels of *yellow* expression uniformly across the wing (Fig. 2D and fig. S3C), the *wing blade* enhancer (26, 28). In an attempt to disentangle the *wing blade* activity from the *spot*-repressing activity, we mapped the latter further with reporter constructs. We found that a 164-base pair (bp) segment adjacent to *peak-1* and devoid of *wing blade* activity

was sufficient to abolish most of the *spot* activity (Fig. 2F). This segment overlapped with a short stretch of differentially accessible DNA between *D. biarmipes* and *D. melanogaster* (fig. S1B, inset).

Together, these results suggest two evolutionary steps that lead to the emergence of a silencer (29), suppressing the *spot* activity in *D. melanogaster*: a gain or increase of accessibility in the region immediately adjacent to the core of the *spot* activity, *spot*¹⁹⁶ (Fig. 1, E and F) (26), and a gain of repressive activity in the newly accessible region. We sought to characterize these events.

Increased accessibility of the *D. melanogaster spot* silencer is promoted by the TF E93, an effector of the ecdysone pathway

We first examined the origin of accessibility of this 164-bp repressive segment. Genome-wide accessibility of regulatory elements in developing wings is governed by the ecdysone pathway (30, 31). Notably, the TF E93, uniformly expressed across the pupal wing (fig. S2E) (31), directly regulates chromatin accessibility at thousands of sites during *D. melanogaster* pupal wing development (30). To test a possible control of E93 on the novel silencer, we depleted E93 from pupal wings using RNA interference (RNAi) (UAS-shE93 and NP3537-Gal4; two independent RNAi lines) and monitored the consequences on *peak-1+164 bp^{mel}* activity. We found that the depletion of E93 was sufficient to restore a *spot* activity with this construct (Fig. 3, B and D; and fig. S2, C and D). Wondering whether this effect was direct, we scanned *peak-1+164 bp^{mel}* with PWMEnrich (32), which uses a similar position weight matrix to that published by Uyehara *et al.* (30) for E93. This scan identified several putative binding sites, including four sites within the 164-bp repressive segment, three of which are not conserved in the orthologous region of spotted species (Fig. 3A and fig. S4). Using a modified version of CUT&RUN (33), we then showed that a tagged version of E93 (E93^{GSTF}) (30) bound upstream of *yellow* transcription start site while the *spot* activity was being repressed. In particular, a small peak of E93 binding centered on the 164-bp repressive segment in phase with a peak of accessibility and a peak of H3K27ac, a mark for active regulatory elements (Fig. 3D and fig. S1D) (34). This was consistent with chromatin immunoprecipitation sequencing data showing that E93 binds to the region of peak-2 in 24-hour after puparium formation (APF) pupal wings (fig. S1D) (30). Last, to clarify the exact role of E93 in the repression of the *spot* activity, we examined previously published E93 Formaldehyde-Assisted Isolation of Regulatory Elements (FAIRE)-seq data on pupal wings from (30) (at 44% of pupal development, somewhat earlier than the stages we have studied with ATAC-seq). We found that the region of peak-2 at the *yellow* locus of *D. melanogaster* had a markedly reduced accessibility in E93 mutants compared to wild type (fig. S1D). We concluded from these experiments that the accessibility to the *spot*-repressive segment was granted by the ecdysone pathway effector E93, presumably directly.

Because the *spot* enhancer, both the cryptic version of *D. melanogaster* (*peak-1^{mel}*) and the active version of *D. biarmipes*, is regulated by the spatial regulator Dll, we were intrigued by previous work showing a genetic interaction between these two factors (35). In the context of touch organ development on fly legs, E93 has a permissive role, enabling the expression and action of Dll and thereby the formation of bracts, cuticular productions at the base of sensory bristles. Although this work did not examine the molecular mode of action of E93 in bract cells, its conclusion is

perfectly consistent with the permissive role of E93 that we uncovered at the *yellow* locus. It also hints at a possible direct partnership between E93 and Dll.

Repression of the *spot* activity likely evolved through splicing within the newly accessible region

Turning to the repressive activity proper, we noticed that the *spot*-repressive segment of *D. melanogaster* had sequence gaps in the vicinity of putative E93 TFBSs, compared to the orthologous segments of the spotted species *D. biarmipes* and *Drosophila suzukii* (Fig. 4A). While the exact position of these indels depended on sequence alignment parameters, they nevertheless resulted in sequence splicing in *D. melanogaster* at two positions (site 1 and site 2; Fig. 4A) in comparison to other species. We reasoned that such splicing might have created TFBSs for repressors and tested this possibility with point mutations at the spliced sites. A mutation of the first candidate repressor site (*peak-1+164 bp^{mel} KO site 1*) resulted in a weak but clear derepression of the cryptic *spot* activity (Fig. 4, B, C, and E), while a mutation of the second site (*peak-1+164 bp^{mel} KO site 2*) did not lead to derepression (Fig. 4, B, D, and E). In summary, our data suggest that the *spot* activity of *D. melanogaster* is constitutively silenced through sites for an unidentified repressor, located within a 164-bp DNA segment adjacent to the core *spot*¹⁹⁶, and accessible in pupal wings.

DISCUSSION

The results presented here show a direct involvement of chromatin accessibility changes to regulatory and morphological evolution (Fig. 4F). We propose that, along with the gains and losses of TFBS for spatial regulators, modulation of enhancer accessibility constitutes a level of phenotypic diversification that may have been overlooked. Genome-wide analyses among ecotypes of the plant *Arabidopsis thaliana* suggested, for instance, that most divergences in accessibility of regulatory regions were not associated with changes in gene expression (36); likewise, a comparative survey of accessibility changes between two yeast species concluded that changes in accessibility might have modest consequences on gene regulation (37). It is conceivable that the contribution of accessibility changes to regulatory evolution is difficult to assess, because the functional significance of accessibility peaks is not necessarily proportional to peak size and might be biased by peak-calling procedures.

Rather than an enhancer decay or deletion (8, 38), the evolutionary mechanism that led to the loss of activity of an enhancer of the pigmentation gene *yellow* is convoluted and implies several evolutionary steps (Fig. 4F). The silenced *spot* activity represents cryptic variation (39) potentially available for the reemergence of a pigmentation spot or perhaps expressed under certain environmental conditions or genomic background. Epigenetic changes have been shown to affect pigmentation through the modification of accessibility of specific regulatory regions in response to temperature changes (40).

In terms of mutational path and likelihood (41), the activity of an enhancer may be lost through direct mutations in its TFBSs, rather than repressed by the emergence of a new *cis*-regulatory element. The former situation has been abundantly documented in insects and in vertebrates (7–9, 42–44). A rare and interesting exception involves the gain of a repressor TFBS leading to enhancer silencing

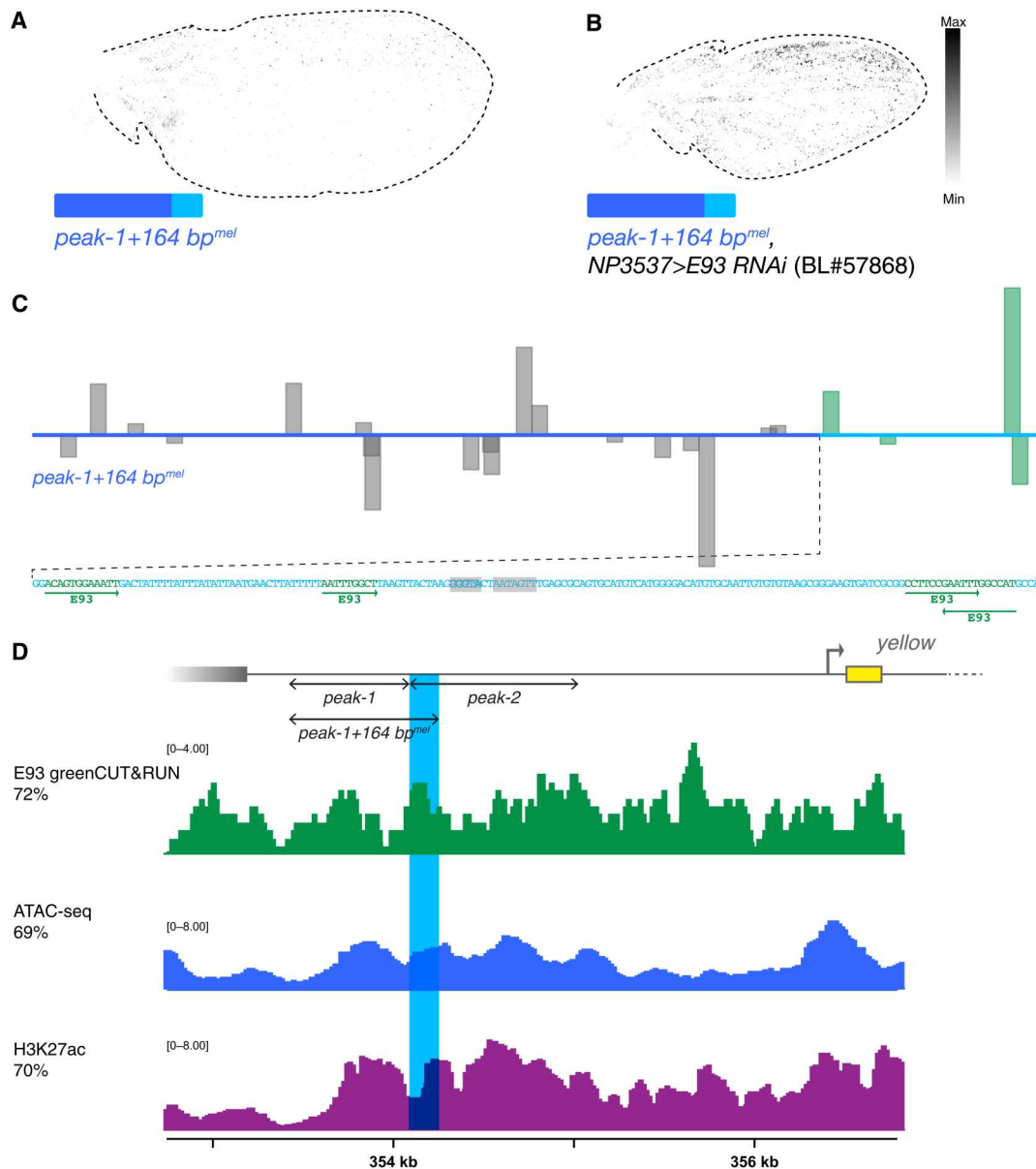


Fig. 3. The ecdysone effector E93 regulates accessibility of a novel silencer at the *D. melanogaster yellow* locus. (A and B) The *spot*-repressing activity (A) is reduced when depleting E93 from pupal wings by means of RNA interference (RNAi) (B). The knockdown of E93 function also affects general wing development in this line, resulting in deformed wings. (C) Predicted E93 sites and their relative binding affinities (proportional to bar lengths) along *peak-1+164 bp^{mel}* [based on the binding motif defined in (30)]. Note that the predicted repressive segment mapped in Fig. 2 contains four putative E93 binding sites, highlighted in green. (D) E93 binds to the 164-bp repressive segment. A greenCUT&RUN experiment (33) shows a peak of E93 binding phased with a small peak of accessibility and marks for active regulatory elements (H3K27ac) centered on the 164-bp repressive segment (turquoise blue). Wings in (A) and (B) are heterozygous for the transgene, and both images were enhanced using the same settings, which differ from those used in other figures.

(45). These different studies, however, did not examine whether accessibility had changed along with the reduced or lost enhancer activity. It is conceivable that when an enhancer accumulates mutations in TFBSs for activators, it also accumulates changes in sites regulating accessibility, but these accessibility sites may be mutated first, corresponding to the onset of enhancer decay.

The situation that we observed in *D. melanogaster*, however, requires a more complex explanation. One possibility is that the silencing of the *spot* evolved by serendipity and was rapidly fixed,

for instance, under sexual selection from females preferring non-spotted males. Alternatively, the entangled regulatory structure of *yellow* in spotted species (26) may have constrained the mutational path to losing the *spot* activity through silencing. For reasons that remain elusive, the direct mutation of *spot* activator sites may not have been permissible in terms of natural selection, for instance, because of pleiotropic effects on the *wing blade* activity. The emergence of a silencer may have offered an alternative route,

melanogaster Canton S (cultured at 20°C); *D. melanogaster* UAS-E93 RNAi lines P{TRiP.HMC04773}attP40 (Bloomington, no. 57868) and KK108140 (Vienna *Drosophila* Resource Center, no. V104390) (47); *D. melanogaster* UAS-Dll RNAi line (Bloomington, no. 29337); *D. melanogaster* protein trap line E93^{GFSTF} (Bloomington, no. 43675) (30); NP3537, tub-GAL80^{ts} [wing-specific Gal4 driver combined to a thermosensitive Gal80 repressor (48)]; and *D. melanogaster* line D2 (26). All UAS RNAi lines were driven by the wing-specific Gal4 driver NP3537 (48) and cultured at 25°C, where Gal4 is repressed by a tub-GAL80^{ts} transgene. Selected wandering third instar larvae or white pre-pupae were transferred to 29°C and imaged 72 to 75 hours later. Pupal stages are expressed in percentage of pupal development, where white pre-pupae correspond to 0% and flies about to emerge from the pupal case correspond to 100%. This establishes a unique scale for staging pupae from different species, with pupal life of slightly different durations or pupae raised at different temperatures. Wings for genomic experiments were dissected either on microscope slides (for pupae older than 60%) or in cold phosphate-buffered saline (PBS) (for pupae younger than 60%) and rinsed in cold PBS following previous descriptions (49, 50).

Transgenesis

All reporter constructs were injected as described in Arnoult *et al.* (23). We used ϕ C31-mediated transgenesis (51) and integrated all constructs at the genomic *attP* site *VK00016* (*attP* line; Bloomington, no. 9735) on chromosome 2 (52). The enhancer sequence of all transgenic stocks was genotyped before imaging. The sequences of all fragments that we tested are provided in table S1. All primers are listed in table S2.

Molecular biology

Constructs for enhancer-reporter assay were cloned as described before (26) with some modifications. PCR-amplified fragments derived from *D. biarmipes* and *D. melanogaster* genomic strains used for ATAC-seq were cloned into pRedSA digested with Eco RI and Bam HI, using the T4 ligase (New England Biolabs, USA). Chimeric constructs were stitched using type IIS restriction enzyme cloning. The 164-bp fragments with mutations were synthesized by Integrated DNA Technologies (USA) with adaptors for type IIS restriction enzymes and then cloned into pRedSA.

ATAC-seq

ATAC-seq was performed as described in Xin *et al.* (26) with modifications. For nuclei preparation: Dissected wings were immediately moved into cold 1× lysis buffer after rinsing. Twenty-four 0% pupal development wing discs, 14 to 17 wings from at least 11 individuals at 47% pupal development, and 24 wings from later stages were used for the following steps, respectively. Only the pupal wings older than 60% of pupal development were cut before disruption. Samples were incubated on ice for 20 to 30 min before and after disruption. For tagmentation: The reaction was set up with 18 μ l of Tagment DNA Buffer (Illumina, no. 15027866) with nuclei plus 2 μ l of Tagment DNA Enzyme (Illumina, no. 15027865). ATAC-seq library preparation and sequencing were performed as described in Xin *et al.* (26), with two replicates per stage (biological replicates). ATAC-seq libraries were then processed as described in Xin *et al.* (26) until peak calling. Normalized bedGraph files were then generated from two merged replicates using MACS2 with the

following settings: --keep-dup all; -q 0.01; --nomodel; --shift -100; --extsize 200; -B --SPMR. Peak calling was performed using HOMER (53) with the following settings: -style histone -size 100 -minDist 100 -gsize 1.2e+8 -o auto.

CUT&RUN

We adapted the manufacturer's protocol (EpiCypher, Chapel Hill, USA) in the following subsections.

Buffers

1× PBS with 6 mM MgCl₂; ATAC-seq 1× lysis buffer; cross-link buffer: 10 mM Hepes (pH 8.0), 100 mM NaCl, 1 mM EDTA (pH 8.0), 0.5 mM EGTA (pH 8.0), and 0.1% formaldehyde (Sigma-Aldrich, F1635); 2.5 M glycine in 1× PBS; quench solution: 1× PBS, 125 mM glycine, and 0.1% Triton X-100. Other buffers follow EpiCypher protocol, including bead activation buffer, cross-link (XL) prewash buffer, XL wash buffer (WB), digitonin buffer with 0.01% digitonin, antibody buffer, and stop buffer.

Cell preparation

Thirty-five to 45 wings per biological replicate at 67% pupal development from *D. melanogaster* line D2 (26) were transferred into a 5-ml Eppendorf tube with cold 1× PBS with 6 mM MgCl₂, rocked at 4°C with 1× cold lysis buffer for 5 min, and then lightly cross-linked (1 min) with the cross-link buffer. The wings were then rocked at room temperature for 1 min and immediately quenched with glycine, transferred into a glass well with 50 μ l of cold XL WB buffer, and cut coarsely (three pieces per wing). Homogenization was performed with a 2-ml dounce using pestle A for 12 strokes and then pestle B for 30 strokes. The homogenate was incubated on ice for 40 to 50 min and then centrifuged at 1000g for 10 min at 4°C with an addition of 500 μ l of XL WB. The nuclei pellet was resuspended with 100 μ l of XL WB and processed for CUT&RUN.

CUT&RUN against H3K27ac

We followed instructions from EpiCypher, including bead activation, binding cells to activated beads, binding of antibodies, binding of Protein A and G fused to Micrococcal Nuclease (pAG-MNase), targeted chromatin digestion and release, and reverse cross-linking. DNA was then purified with QIAGEN MinElute kit and subsequently processed for library preparation. One microliter of antibody against H3K27ac (Active Motif, no. 39034) was used. Two biological replicates were done.

greenCUT&RUN against E93

Cells were prepared as described above for canonical CUT&RUN with minor modifications. Seventy to 90 pupal wings (72% pupal development) per replicate from E93 protein trap (Bloomington, no. 43675) were used for the experiment (two biological replicates were done). The wings were rocked at room temperature for 4 min for cross-link, instead of a 1-min light cross-link. We then followed the protocol from Koidl *et al.* (33) until the DNA isolation step. The concentration of digitonin in the digitonin buffer was 0.05%. Reverse cross-link and DNA isolation were done as described above for CUT&RUN against H3K27ac. The DNA was then processed for library preparation. MNase-coupled green fluorescent protein nanobodies were from M. Timmers.

Library preparation, sequencing, and data analysis

For both CUT&RUN and greenCUT&RUN, we used the NEBNext Ultra II DNA Library Prep Kit for Illumina and NEBNext Multiplex Oligos for Illumina (Dual Index Primers Set 2) for library construction, following the protocol from Liu (54). Sequencing was done as in Xin *et al.* (26). The sequencing depth is 5 to 10 million reads per

library. Demultiplexed and trimmed libraries were aligned to the reference genome UCSC (University of California, Santa Cruz) dm6 using Bowtie2 (55, 56) with parameters from Meers *et al.* (57): --end-to-end --very-sensitive --no-mixed --no-discordant -q --phred33 -I 10 -X 700. The aligned reads were filtered and cleaned as described for ATAC-seq in (26). Peak calling was done by MACS2 (58) with the following settings: -f BAMPE --keep-dup all -q 0.01 -g 1.2e+8 -B --SPMR.

yellow RNA quantification

RNA extraction

Ten to 12 wings from at least 7 individuals (earlier than 60% of pupal development) and 15 to 20 wings from at least 10 individuals (older than 60% of pupal development) were dissected, rinsed twice in cold PBS, and then transferred into ~150 μ l of RLT buffer (QIAGEN) with β -mercaptoethanol and stored at -80°C until further processing. Before performing RNA extraction, each sample was brought up to 350 μ l with RLT buffer and transferred into tubes with 2.38-mm metal beads (QIAGEN PowerBead). The wings were homogenized using a microtube homogenizer (BeadBug) for 50 s, power at 400, repeated once. The following steps were performed on the basis of the QIAGEN RNeasy Kit protocol. The RNA was then treated with deoxyribonuclease I (M0303S, New England Biolabs, USA) and then cleaned up using the Monarch RNA Cleanup kit (New England Biolabs, USA). The following stages were selected for RNA extraction: 30, 56, 61, 70, 77, and 86% of pupal development.

RT-PCR

cDNA was synthesized using ProtoScript II First Strand cDNA Synthesis Kit (New England Biolabs, USA) following the manufacturer's instructions. Six microliters of RNA was used for cDNA synthesis. Reverse transcription PCR (RT-PCR) was performed using Phusion High-Fidelity DNA Polymerase (New England Biolabs, USA), and cDNA was synthesized as above. Primers used for RT-PCR are described in Table S2. RT-PCR products were checked on 1.3% agarose gel.

Quantitative real-time PCR

Quantitative real-time PCR was performed using Phusion High-Fidelity DNA Polymerase (New England Biolabs, USA) and SYBR Green I Nucleic Acid Gel Stain (Invitrogen), and cDNA was generated as described above. The expression levels of *Actin 42A* at each time point was used as an internal control. The primers were the same as the ones used for RT-PCR. The Ct values were measured by the Bio-Rad CFX Connect Real-Time PCR Detection System, and the Ct values from technical duplicates and biological duplicates were averaged for relative expression calculation.

Imaging

Sample preparation and microscopy

All transgenic wings imaged in this study were homozygous for the reporter construct, unless otherwise stated. Male white pre-pupae were left to develop for 90 to 92 hours at 25°C . Pupal wings were dissected as described above, transferred into water to unfold them, then mounted in PBS on a microscope slide with a coverslip, and immediately imaged with a Ti2-Eclipse Nikon microscope. All images were acquired as in Xin *et al.* (26).

Fluorescence quantification

z stacks were projected using Fiji (59) with maximum intensity. Projected images were further processed in MATLAB to generate masks

segmenting nuclei with fluorescent signal. Specifically, a Gaussian high-pass filter was used to detect and segment nuclei before generating nuclei binary masks. These masks were then used to measure image intensity in Fiji. At least seven individual wings were measured for each construct. In Fig. 2I, the degree of repression of *spot* activity was measured as the ratio of average fluorescence (overall intensity/area) between two areas of the wing: The region comprised between veins L2 and L3 and the region posterior to vein L5. The former is the region where *spot* activity is modulated, and the latter is a reference for uniform *wing blade* activity. For each wing image, the region between L2 and L3 as well as the region posterior to L5 were selected manually, and the mean intensity of each was measured using the masks described above. In Fig. 4E, the overall intensity of the region between L2 and L3 was measured after applying a mask segmenting the nuclei but was not compared to the region posterior to L5 as above, as these constructs are devoid of *wing blade* activity. The number of nuclei per wing, counted using different reporter lines with expression across the wing, does not vary much in this genetic background ($12,392 \pm 889$; $n = 36$) and is not likely to bias the overall intensity signal.

Image enhancement

Images in the figures were enhanced for visual clarity in agreement with the journal image integrity standards, exclusively with linear adjustments.

E93 motif search

Software from Bioconductor, PWMEnrich (32), was used for motif scan. A built-in motif database for *Drosophila* was used for scanning motifs. "Eip93F_SANGER_10_FBgn0013948" was used for plotting E93 binding sites on *yellow* sequences (*peak-1+164 bp^{mel}*; Fig. 3C).

Multisequence alignment

Multisequence alignment was performed with MULTiple Sequence Comparison by Log-Expectation (MUSCLE) from European Molecular Biology Laboratory-European Bioinformatics Institute (EMBL-EBI) online tools (60) using default settings. All sequences from *yellow* upstream regulatory regions are from the reference genomes of *D. sukukii*, *D. melanogaster*, and *D. biarmipes* and listed in table S1 as *y 5' full^{suz}*, *y 5' full^{mel}*, and *y 5' full^{bia}*, respectively.

Supplementary Materials

This PDF file includes:

Figs. S1 to S4

Legends for tables S1 and S2

Other Supplementary Material for this

manuscript includes the following:

Tables S1 and S2

[View/request a protocol for this paper from Bio-protocol.](#)

REFERENCES AND NOTES

1. S. B. Carroll, From pattern to gene, from gene to pattern. *Int. J. Dev. Biol.* **42**, 305–309 (1998).
2. P. Piazza, C. D. Bailey, M. Cartolano, J. Krieger, J. Cao, S. Ossowski, K. Schneeberger, F. He, J. de Meaux, N. Hall, N. Macleod, D. Filatov, A. Hay, M. Tsiantis, *Arabidopsis thaliana* leaf form evolved via loss of KNOX expression in leaves in association with a selective sweep. *Curr. Biol.* **20**, 2223–2228 (2010).

3. M. D. Shapiro, M. E. Marks, C. L. Peichel, B. K. Blackman, K. S. Nereng, B. Jonsson, D. Schluter, D. M. Kingsley, Genetic and developmental basis of evolutionary pelvic reduction in threespine sticklebacks. *Nature* **428**, 717–723 (2004).
4. E. Sucena, I. Delon, I. Jones, F. Payre, D. L. Stern, Regulatory evolution of shavenbaby/ovo underlies multiple cases of morphological parallelism. *Nature* **424**, 935–938 (2003).
5. S. B. Carroll, Evo-devo and an expanding evolutionary synthesis: A genetic theory of morphological evolution. *Cell* **134**, 25–36 (2008).
6. S. J. Adamowicz, A. Purvis, From more to fewer? Testing an allegedly pervasive trend in the evolution of morphological structure. *Evolution* **60**, 1402–1416 (2006).
7. E. Z. Kvon, O. K. Kamneva, U. S. Melo, I. Barozzi, M. Osterwalder, B. J. Mannion, V. Tissieres, C. S. Pickle, I. Plajzer-Frick, E. A. Lee, M. Kato, T. H. Garvin, J. A. Akiyama, V. Afzal, J. Lopez-Rios, E. M. Rubin, D. E. Dickel, L. A. Pennacchio, A. Visel, Progressive loss of function in a limb enhancer during snake evolution. *Cell* **167**, 633–642.e11 (2016).
8. B. Prud'homme, N. Gompel, A. Rokas, V. A. Kassner, T. M. Williams, S. D. Yeh, J. R. True, S. B. Carroll, Repeated morphological evolution through cis-regulatory changes in a pleiotropic gene. *Nature* **440**, 1050–1053 (2006).
9. N. Frankel, D. F. Erezilymaz, A. P. McGregor, S. Wang, F. Payre, D. L. Stern, Morphological evolution caused by many subtle-effect substitutions in regulatory DNA. *Nature* **474**, 598–603 (2011).
10. M. Z. Ludwig, C. Bergman, N. H. Patel, M. Kreitman, Evidence for stabilizing selection in a eukaryotic enhancer element. *Nature* **403**, 564–567 (2000).
11. M. Z. Ludwig, A. Palsson, E. Alekseeva, C. M. Bergman, J. Nathan, M. Kreitman, Functional evolution of a cis-regulatory module. *PLoS Biol.* **3**, e93 (2005).
12. M. Levine, Transcriptional enhancers in animal development and evolution. *Curr. Biol.* **20**, R754–R763 (2010).
13. E. E. Hare, B. K. Peterson, M. B. Eisen, A careful look at binding site reorganization in the even-skipped enhancers of *Drosophila* and sepsids. *PLoS Genet.* **4**, e1000268 (2008).
14. D. Papatsenko, Y. Goltsev, M. Levine, Organization of developmental enhancers in the *Drosophila* embryo. *Nucleic Acids Res.* **37**, 5665–5677 (2009).
15. J. Pu, Z. Wang, H. Cong, J. S. R. Chin, J. Justen, C. Finet, J. Y. Yew, H. Chung, Repression precedes independent evolutionary gains of a highly specific gene expression pattern. *Cell Rep.* **37**, 109896 (2021).
16. D. J. McKay, J. D. Lieb, A common set of DNA regulatory elements shapes *Drosophila* appendages. *Dev. Cell* **27**, 306–318 (2013).
17. D. Shlyueva, G. Stampfel, A. Stark, Transcriptional enhancers: From properties to genome-wide predictions. *Nat. Rev. Genet.* **15**, 272–286 (2014).
18. M. Bozkek, N. Gompel, Developmental transcriptional enhancers: A subtle interplay between accessibility and activity. *Bioessays* **42**, e1900188 (2020).
19. L. A. Cirillo, F. R. Lin, I. Cuesta, D. Friedman, M. Jarnik, K. S. Zaret, Opening of compacted chromatin by early developmental transcription factors HNF3 (FoxA) and GATA-4. *Mol. Cell* **9**, 279–289 (2002).
20. J. Jacobs, M. Atkins, K. Davie, H. Imrichova, L. Romanelli, V. Christiaens, G. Hulselms, D. Potier, J. Wouters, I. I. Taskiran, G. Paciello, C. B. González-Blas, D. Koldere, S. Aibar, G. Halder, S. Aerts, The transcription factor *Grainy head* primes epithelial enhancers for spatiotemporal activation by displacing nucleosomes. *Nat. Genet.* **50**, 1011–1020 (2018).
21. Y. Sun, C.-Y. Nien, K. Chen, H.-Y. Liu, J. Johnston, J. Zeitlinger, C. Rushlow, Zelda overcomes the high intrinsic nucleosome barrier at enhancers during *Drosophila* zygotic genome activation. *Genome Res.* **25**, 1703–1714 (2015).
22. P. C. Peng, P. Khoueir, C. Girardot, J. P. Reddington, D. A. Garfield, E. E. M. Furlong, S. Sinha, The role of chromatin accessibility in cis-regulatory evolution. *Genome Biol. Evol.* **11**, 1813–1828 (2019).
23. L. Arnault, K. F. Su, D. Manoel, C. Minervino, J. Magrina, N. Gompel, B. Prud'homme, Emergence and diversification of fly pigmentation through evolution of a gene regulatory module. *Science* **339**, 1423–1426 (2013).
24. N. Gompel, B. Prud'homme, P. J. Wittkopp, V. A. Kassner, S. B. Carroll, Chance caught on the wing: Cis-regulatory evolution and the origin of pigment patterns in *Drosophila*. *Nature* **433**, 481–487 (2005).
25. Y. Le Poul, Y. Xin, L. Ling, B. Muhling, R. Jaenichen, D. Horl, D. Bunk, H. Harz, H. Leonhardt, Y. Wang, E. Osipova, M. Museridze, D. Dharmadhikari, E. Murphy, R. Rohs, S. Preibisch, B. Prud'homme, N. Gompel, Regulatory encoding of quantitative variation in spatial activity of a *Drosophila* enhancer. *Sci. Adv.* **6**, eabe2955 (2020).
26. Y. Xin, Y. Le Poul, L. Ling, M. Museridze, B. Muhling, R. Jaenichen, E. Osipova, N. Gompel, Ancestral and derived transcriptional enhancers share regulatory sequence and a pleiotropic site affecting chromatin accessibility. *Proc. Natl. Acad. Sci. U.S.A.* **117**, 20636–20644 (2020).
27. J. D. Buenrostro, B. Wu, H. Y. Chang, W. J. Greenleaf, ATAC-seq: A method for assaying chromatin accessibility genome-wide. *Curr. Protoc. Mol. Biol.* **109**, 21.29.21–221.29.9 (2015).
28. P. J. Wittkopp, K. Vaccaro, S. B. Carroll, Evolution of *yellow* gene regulation and pigmentation in *Drosophila*. *Curr. Biol.* **12**, 1547–1556 (2002).
29. S. Ogbourne, T. M. Antalis, Transcriptional control and the role of silencers in transcriptional regulation in eukaryotes. *Biochem. J.* **331**, 1–14 (1998).
30. C. M. Uyehara, S. L. Nystrom, M. J. Niederhuber, M. Leatham-Jensen, Y. Ma, L. A. Buttitta, D. J. McKay, Hormone-dependent control of developmental timing through regulation of chromatin accessibility. *Genes Dev.* **31**, 862–875 (2017).
31. S. L. Nystrom, M. J. Niederhuber, D. J. McKay, Expression of E93 provides an instructive cue to control dynamic enhancer activity and chromatin accessibility during development. *Development* **147**, dev181909 (2020).
32. R. Stojnic, D. Diez, PWMEnrich: PWM enrichment analysis. *R package*, (2021).
33. S. Koidl, H. T. M. Timmers, greenCUT&RUN: Efficient genomic profiling of GFP-tagged transcription factors and chromatin regulators. *Curr. Protoc.* **1**, e266 (2021).
34. M. P. Creighton, A. W. Cheng, G. G. Welstead, T. Kooistra, B. W. Carey, E. J. Steine, J. Hanna, M. A. Lodato, G. M. Frampton, P. A. Sharp, L. A. Boyer, R. A. Young, R. Jaenisch, Histone H3K27ac separates active from poised enhancers and predicts developmental state. *Proc. Natl. Acad. Sci. U.S.A.* **107**, 21931–21936 (2010).
35. X. Mou, D. M. Duncan, E. H. Baehrecke, I. Duncan, Control of target gene specificity during metamorphosis by the steroid response gene E93. *Proc. Natl. Acad. Sci. U.S.A.* **109**, 2949–2954 (2012).
36. C. M. Alexandre, J. R. Urton, K. Jean-Baptiste, J. Huddleston, M. W. Dorrry, J. T. Cuperus, A. M. Sullivan, F. Bemm, D. Jolic, A. A. Arsovski, A. Thompson, J. L. Nemhauser, S. Fields, D. Weigel, K. L. Bubb, C. Queitsch, Complex relationships between chromatin accessibility, sequence divergence, and gene expression in *Arabidopsis thaliana*. *Mol. Biol. Evol.* **35**, 837–854 (2018).
37. C. F. Connelly, J. Wakefield, J. M. Akey, Evolution and genetic architecture of chromatin accessibility and function in yeast. *PLoS Genet.* **10**, e1004427 (2014).
38. Y. F. Chan, M. E. Marks, F. C. Jones, G. Villarreal Jr., M. D. Shapiro, S. D. Brady, A. M. Southwick, D. M. Absher, J. Grimwood, J. Schmutz, R. M. Myers, D. Petrov, B. Jonsson, D. Schluter, M. A. Bell, D. M. Kingsley, Adaptive evolution of pelvic reduction in sticklebacks by recurrent deletion of a Pitx1 enhancer. *Science* **327**, 302–305 (2010).
39. P. J. Polaczyk, R. Gasperini, G. Gibson, Naturally occurring genetic variation affects *Drosophila* photoreceptor determination. *Dev. Genes Evol.* **207**, 462–470 (1998).
40. J. M. Gibert, E. Mouchel-Vielh, S. De Castro, F. Peronnet, Phenotypic plasticity through transcriptional regulation of the evolutionary hotspot gene tan in *Drosophila melanogaster*. *PLoS Genet.* **12**, e1006218 (2016).
41. N. Gompel, B. Prud'homme, The causes of repeated genetic evolution. *Dev. Biol.* **332**, 36–47 (2009).
42. O. Nagy, I. Nuez, R. Savisaar, A. E. Peluffo, A. Yassin, M. Lang, D. L. Stern, D. R. Matute, J. R. David, V. Courtier-Orgogozo, Correlated evolution of two copulatory organs via a single cis-regulatory nucleotide change. *Curr. Biol.* **28**, 3450–3457.e13 (2018).
43. F. Leal, M. J. Cohn, Loss and re-emergence of legs in snakes by modular evolution of sonic hedgehog and HOXD enhancers. *Curr. Biol.* **26**, 2966–2973 (2016).
44. C. A. Guenther, B. Tasic, L. Luo, M. A. Bedell, D. M. Kingsley, A molecular basis for classic blond hair color in Europeans. *Nat. Genet.* **46**, 748–752 (2014).
45. E. Preger-Ben Noon, F. P. Davis, D. L. Stern, Evolved repression overcomes enhancer robustness. *Dev. Cell* **39**, 572–584 (2016).
46. Z. X. Chen, D. Sturgill, J. Qu, H. Jiang, S. Park, N. Boley, A. M. Suzuki, A. R. Fletcher, D. C. Plachetzki, P. C. FitzGerald, C. G. Artieri, J. Atallah, O. Barmina, J. B. Brown, K. P. Blankenburg, E. Clough, A. Dasgupta, S. Gubbala, Y. Han, J. C. Jayaseelan, D. Kalra, Y. A. Kim, C. L. Kovar, S. L. Lee, M. Li, J. D. Malley, J. H. Malone, T. Mathew, N. R. Mattiuzzo, M. Munidasa, D. M. Muzny, F. Onger, L. Perales, T. M. Przytycka, L. L. Pu, G. Robinson, R. L. Thornton, N. Saada, S. E. Scherer, H. E. Smith, C. Vinson, C. B. Warner, K. C. Worley, Y. Q. Wu, X. Zou, P. Cherbas, M. Kellis, M. B. Eisen, F. Piano, K. Kionte, D. H. Fitch, P. W. Sternberg, A. D. Cutter, M. O. Duff, R. A. Hoskins, B. R. Graveley, R. A. Gibbs, P. J. Bickel, A. Kopp, P. Carninci, S. E. Celniker, B. Oliver, S. Richards, Comparative validation of the *D. melanogaster* modENCODE transcriptome annotation. *Genome Res.* **24**, 1209–1223 (2014).
47. M. C. Pahl, S. E. Doyle, S. E. Siegrist, E93 integrates neuroblast intrinsic state with developmental time to terminate MB neurogenesis via autophagy. *Curr. Biol.* **29**, 750–762.e3 (2019).
48. A. Pavlopoulos, M. Akam, Hox gene Ultrathorax regulates distinct sets of target genes at successive stages of *Drosophila* haltere morphogenesis. *Proc. Natl. Acad. Sci. U.S.A.* **108**, 2855–2860 (2011).
49. C. Bolatto, C. Parada, V. Colmenares, A rapid and efficient method to dissect pupal wings of *Drosophila* suitable for immunodetections or PCR assays. *J. Vis. Exp.*, 55854 (2017).
50. K. Flegel, D. Sun, O. Grushko, Y. Ma, L. Buttitta, Live cell cycle analysis of *Drosophila* tissues using the attune acoustic focusing cytometer and vybrant dyecycle violet DNA stain. *J. Vis. Exp.*, e50239 (2013).

51. A. Groth, M. Fish, R. Nusse, M. Calos, Construction of transgenic *Drosophila* by using the site-specific integrase from phage phiC31. *Genetics* **166**, 1775–1782 (2004).
52. K. J. Venken, Y. He, R. A. Hoskins, H. J. Bellen, P[acman]: A BAC transgenic platform for targeted insertion of large DNA fragments in *D. melanogaster*. *Science* **314**, 1747–1751 (2006).
53. S. Heinz, C. Benner, N. Spann, E. Bertolino, Y. C. Lin, P. Laslo, J. X. Cheng, C. Murre, H. Singh, C. K. Glass, Simple combinations of lineage-determining transcription factors prime cis-regulatory elements required for macrophage and B cell identities. *Mol. Cell* **38**, 576–589 (2010).
54. N. Liu, *Library Prep for CUT&RUN with NEBNext® Ultra™ II DNA Library Prep Kit for Illumina® (E7645)* (2021); www.protocols.io.
55. B. Langmead, S. L. Salzberg, Fast gapped-read alignment with Bowtie 2. *Nat. Methods* **9**, 357–359 (2012).
56. B. Langmead, C. Wilks, V. Antonescu, R. Charles, Scaling read aligners to hundreds of threads on general-purpose processors. *Bioinformatics* **35**, 421–432 (2019).
57. M. P. Meers, T. D. Bryson, J. G. Henikoff, S. Henikoff, Improved CUT&RUN chromatin profiling tools. *eLife* **8**, e46314 (2019).
58. Y. Zhang, T. Liu, C. A. Meyer, J. Eeckhoutte, D. S. Johnson, B. E. Bernstein, C. Nusbaum, R. M. Myers, M. Brown, W. Li, X. S. Liu, Model-based analysis of ChIP-Seq (MACS). *Genome Biol.* **9**, R137 (2008).
59. J. Schindelin, I. Arganda-Carreras, E. Frise, V. Kaynig, M. Longair, T. Pietzsch, S. Preibisch, C. Rueden, S. Saalfeld, B. Schmid, J. Y. Tinevez, D. J. White, V. Hartenstein, K. Eliceiri, P. Tomancak, A. Cardona, Fiji: An open-source platform for biological-image analysis. *Nat. Methods* **9**, 676–682 (2012).
60. F. Madeira, M. Pearce, A. R. N. Tivey, P. Basutkar, J. Lee, O. Edbali, N. Madhusoodanan, A. Kolesnikov, R. Lopez, Search and sequence analysis tools services from EMBL-EBI in 2022. *Nucleic Acids Res.* **50**, W276–W279 (2022).

Acknowledgments: We thank A. Maugarny-Calès and M. Timmers for sharing stocks and reagents. We are grateful to B. Prud'homme and S. Ceolin for constructive comments on the manuscript, to V. Courtier for advice on the literature, to L. Osipova for assistance with fly maintenance, to Y. Xin for help with sample collection, and to S. Feng for technical advice.

Funding: This work was supported by the Graduate School of Quantitative Biosciences Munich (QBM; to L.L.), the Human Frontiers Science Program (program grant RGP0021/2018 to N.G.), and the Deutsche Forschungsgemeinschaft (grants INST 86/1783-1 LAGG, GO 2495/5-1, and GO 2495/11-1 to N.G.). **Author contributions:** L.L. and N.G. conceptualized the project. L.L. designed all experiments and performed all RNA-related, genomic, and imaging experiments and all data analysis. B.M. produced all transgenic lines. R.J. performed all other molecular biology experiments. L.L. and N.G. analyzed and interpreted the data. N.G. wrote the manuscript, which L.L. edited. N.G. supervised the project and acquired funding. **Competing interests:** The authors declare that they have no competing interests. **Data and materials availability:** All data needed to evaluate the conclusions in the paper are present in the paper and/or the Supplementary Materials. All raw and processed ATAC and CUT&RUN sequencing data are available on NCBI Gene Expression Omnibus (GEO; www.ncbi.nlm.nih.gov/geo) through the accession number GSE222717.

Submitted 30 August 2022

Accepted 17 January 2023

Published 17 February 2023

10.1126/sciadv.ade6529